

SAINT ANTHONY CAVE: MORPHOLOGY, GENESIS, AND AGE OF ONE OF THE OLDEST RELIGIOUS SHRINES, SOUTHERN GALALA PLATEAU, EASTERN DESERT, EGYPT

Wafaa Khalaf Fahim¹

Abstract

Saint Anthony Cave is an important cultural, religious, and historic site; it was home of Saint Anthony, one of the earliest Christian monks (ca. 251–356 AD). The cave is located in a *tectonically*-complex karst area developed in partially dolomitic, sandy limestones of latest Paleocene age. Saint Anthony Cave had been described as a phreatic cave in previous research, but the cave lacked a detailed map and its speleogenesis was unclear. New data show the cave is a multi-phased uplifted cave formed primarily under *phreatic* conditions, with later modification by rising water levels. *Deep sources* of dissolutionally aggressive solutions likely have been involved. Speleogenesis likely began in Oligocene time associated with the Gulf of Suez Rift evolution and has been erosionally dissected. New, detailed mapping using ArcGIS shows the cave has an area of 22.13 m² with a length and depth of 17.10 m and 5.33 m, respectively. The cave consists of a northwest–southeast oriented, steeply inclined, fracture controlled, upper-level entrance passage connected to an east–west oriented, fracture controlled, lower-level room with a vertical drop of 2.46 m. Dissolution pockets, cupola-like features, ceiling bell holes, notches, and corrosion tables are present in the cave. Subaerial and subaqueous speleothems moderately decorated the cave with likely Egyptian calcite alabaster. Based on field investigation, regional volcanic and tectonic history, paleoclimates, and other background information, we identify four distinct speleogenetic phases: First, during the late Oligocene, volcanic and extensional tectonic activities fractured the rocks, generated deep-seated acids, and enhanced the rising deep thermal water. Dissolution by other mechanisms such as carbonic/sulfuric acid and mixing dissolution were prevalent. In the early Miocene (Burdigalian), the cave was uplifted. Second, in the late Miocene (about 7.5 Ma), subaerial speleothems were being deposited in the cave under humid climate conditions. Third, post-Miocene, the cave enlarged and modified at and above the water level by likely warm, sulfuric water. Fourth, water levels dropped and speleothems were deposited again during later humid climate conditions.

INTRODUCTION

The presence of dissolution caves is well documented in arid to hyper-arid regions (e.g., Ford and Williams, 2007, and references therein). These caves are mostly inactive relict features, and many have been modified and overprinted by later processes such as dissolution, deposition, and tectonic uplift, obscuring their origin.

Some studies attribute these caves to epigene speleogenesis, where carbonic acid derived from the surface caused speleogenesis (Ford and Williams, 2007). Other caves have no apparent genetic relationship to surface recharge and have certain characteristics suggesting hypogenic speleogenesis.

Hypogenic speleogenesis can result from dissolution mechanisms such as: (1) deep-seated acidic solutions (CO₂/H₂S), (2) cooling thermal water, (3) mixing of waters of contrasting chemistry, such as where deep water mixes with near-surface water or along a freshwater-saltwater contact, (4) sulfuric acid, where H₂S-bearing water interacts with oxygenated shallower water near or above the water table. The last mechanism can take place if both waters are saturated with calcite, but that requires a closed system. H₂S can also be produced by local oxidation of iron sulfides such as pyrite. (Mylroie and Carew, 1990; Palmer, 1991; Palmer, 2007; Dublyansky, 2013; Klimchouk, 2019).

Hypogenic speleogenesis is well documented in arid to hyperarid localities around the world (e.g., Klimchouk et al., 2017). In Egypt, caves that have the characteristics of hypogene caves have been documented in the Southern Galala Plateau (Fahim, 2019). Flank margin caves formed in a freshwater-saltwater contact zone have been documented along the Matruh coast in northwest Egypt (Fahim, 2015).

A BRIEF HISTORY OF SAINT ANTHONY CAVE

Saint Anthony Cave is an important cultural, historic, and religious site. The cave is named after the monk, Saint Anthony the Great, also known as Saint Anthony of Egypt (ca. 251–356 AD). He is considered the first Christian monk and is an important figure among the Desert Fathers and to all of later Christian monasticism.

The cave was the dwelling place of Saint Anthony between approximately 312 and 356 AD. He chose the cave because it was a sanctuary and because of the persistent springs that helped him live in solitude far away from civilization to pursue ascetic ideals. Since his death, Saint Anthony Cave has served as a place for veneration and prayer

¹ Ain Shams University, Cairo, Egypt
e-mail: wafaa-khalaf@hotmail.com

for pilgrims and for visitors from all over the world. A detailed account of the history of the life of Saint Anthony can be found in Rubenson (2016).

Previous Work

The Southern Galala Plateau is also called “El-Galala El-Qibliya” and is located at the northeastern portion of the Eastern Desert of Egypt. The plateau lies at the western shoulder of the Gulf of Suez Rift, a northern extension of Red Sea. Topographically, the plateau is very rugged with a maximum elevation of 1480 m. It is characterized by dry valley (wadi) systems with autogenic recharge (Fig. 1A–C).

The Southern Galala Plateau is tectonically and geologically complex with *highly fractured* carbonate rocks that have surface karst landforms and caves.

Little prior work has been done on caves in the area (Goodman et al., 1992; Hobbs and Goodman, 1995; Halliday, 2000; Halliday, 2001; Halliday, 2003), and there have been few studies of their genesis and ages. A small dissolution cave was located inside the Church of Saint Paul Monastery, but human modification has obscured its location (Lyster, 1999).

Recently work by Fahim (2019) has shown that the Southern Galala Plateau contains a complex and diverse assemblage of karst landforms including karren, caves, residual carbonate hills, dolines, and pocket valleys. This study also discovered and described other karstic caves in the plateau.

The most impressive, newly-discovered cave in the Southern Galala Plateau is Al-Jarf Cave located in the eastern side of the plateau in Wadi Al-Jarf (Al-Jarf Al-Qibli). Al-Jarf Cave is developed in limestone and dolomitic limestone of early Eocene age. The cave is fracture controlled, multilevel, and multi-phased, and it has an area of 1208 m². The cave is at least Oligocene in age. The cave is polygenetic, formed primarily under phreatic and water table settings, likely influenced by deep fluids. Al-Jarf Cave shows 16 types and subtypes of subaerial and subaqueous speleothems with different morphologies, such as stalagmites up to 2.75 m high and 2.10 m in diameter, stalactites, draperies, flowstone, helictites, spar, small raft cones, and others. Deflected stalactites and oriented coralloids are also present. Calcite, gypsum, anhydrite, halite, and other minerals have been identified (Fahim, 2019).

Dissolution caves are present in the northern side of the Southern Galala Plateau and also in the flanks of the wadis. Most have the characteristics of phreatic, water table, epigene caves. Dissolution pockets are the most common features in the caves. Some of the caves contain speleothems. Um Hamada Cave is one of the largest and inaccessible caves and consists of a single large room 1454 m² in area. Some small caves at about 500 m MSL in the northern cliff of the plateau west of the Saint Anthony Monastery are filled with secondary deposits of spar and Egyptian calcite alabaster (see discussion section) (Fahim, 2019).

In the Saint Anthony Monastery, there are some karstic caves, but their origins have been obscured by modification for use as dwellings for monks. Most of the known caves in the area are relict and inactive. In different expeditions, we have discovered other new caves at Wadi Al-Jarf, and condensation-corrosion processes caused by rising vapors are active in one of them (Fahim, 2022). There are extraordinarily unusual, active, large tufa stalactites with a maximum length of about 6 m in Wadi Kharaza, probably fed from active, unopened caves (Fig. 1C).

Saint Anthony Cave was given a brief and useful description by Halliday (2000; 2001; 2003). Halliday gave the dimensions (length, width, height) of the cave but did not map it. Halliday suggested that the cave was formed phreatically

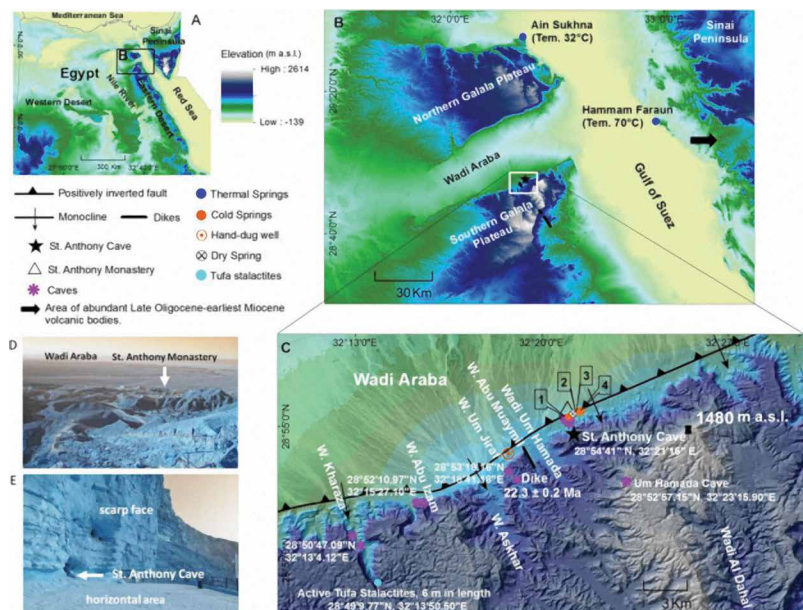


Figure 1. (A) ASTER 90 m-resolution digital elevation model of Egypt. (B) ASTER 90 m resolution digital elevation model showing the location of the Northern and Southern Galala Plateaus. (C) Shaded-relief image of the digital elevation model of the area of Saint Anthony Cave. The inverted fault and the monocline are added according Schütz (1994) and Moustafa and Khalil (1995), respectively. The data and the locations of the volcanic bodies are from Klitzsch et al. (1987), Patton et al. (1994), and Bosworth et al. (2015). Temperatures of the thermal waters are from Sturchio et al. (1996). Numerals 1-4 show springs discussed in the text. Caves are from Fahim (2019). Coordinates for the caves and the tufa stalactites were added according the current study. (D) View of the Saint Anthony Monastery and Wadi Araba near the site of the cave (note people for scale). (E) View in front of Saint Anthony Cave and the nearby area surrounding (note the barrel in the right side of the photo for scale).

and active, large tufa stalactites with a maximum length of about 6 m in Wadi Kharaza, probably fed from active, unopened caves (Fig. 1C).

Saint Anthony Cave was given a brief and useful description by Halliday (2000; 2001; 2003). Halliday gave the dimensions (length, width, height) of the cave but did not map it. Halliday suggested that the cave was formed phreatically

along joints and appeared to be a fossil outflow route. A floor of flowstone, possibly Egyptian alabaster, is located at the cave entrance. There are small phreatic features near the cave. Halliday compared the study area to the North Rim of the Grand Canyon in the USA, where the karstification began in middle Eocene time. Fahim (2019) provided a simple map of the cave and confirmed that the cave had formed at or below the water table.

The aim of this work was to survey the cave and produce a detailed map and to describe the cave morphology in detail, including small dissolution features, and speleothems. This information was used in concert with previous studies on karst development, regional geology, volcanics and tectonics, paleoclimates, and the geologic and hydrologic history of Wadi Araba to determine the physical, structural, and chemical controls on speleogenesis as well as the speleogenetic phases and their relative timing.

LOCATION, CLIMATIC, AND GEOLOGIC SETTING

Saint Anthony Cave (latitude 28°54'41" N, longitude 32°21'16" E, 800 m MSL) opens within the northern cliff of the Southern Galala Plateau (Fig. 1A–C). The cave is currently accessed from the entrance gate of the Saint Anthony Monastery by a 1.5 km walk to a stairway consisting of about 1,400 steps. This stair leads to an unroofed, semi-artificial, horizontal area, 101 m² in area, located in front of the cave and overlooking Wadi Araba and the monastery (Fig. 1D–E).

Proximal to the cave, the scarp face is vertical to overhanging and is highly fractured with joints and normal faults. The scarp face has a corrosion surface with a variety of dissolution features such as small phreatic cavities, hollows with spongework textures, honeycomb-like features, and shallow, flat-roofed notches at localized areas on different levels. Mineral-filled fractures have been observed with some displaying small scalenohedral calcite crystals with different colors. Below the cave, there is a gorge undermined with terraces at different elevations. There are karstified, collapsed rock blocks on the sloped area near the cave. Springs emerge at the foot of the cliff inside the Saint Anthony Monastery.

Climate data for 24 years (1991–2014) was obtained from the Bir Arida meteorological station, located in Wadi Araba at 300 m MSL. The annual average maximum air temperature averaged 29.29 °C over the past 24 years, with individual years ranging between 28.49 °C and 31.35 °C. The annual average minimum air temperature averaged 13.82 °C, ranging between 12.57 °C and 15.20 °C. The annual average daily air temperature averaged 23.36 °C, ranging between 22.13 °C and 24.80 °C. The average daily air temperature ranged between 10.9 °C and 22.4 °C in winter and averaged between 27.4 °C and 33.5 °C in summer.

The highest average monthly maximum temperature was 37.27 °C in July, while the lowest average monthly minimum temperature was 5.16 °C in January. The total amount of annual rainfall ranged between 0 and 14.3 mm. The inland area of the Southern Galala Plateau and Wadi Araba is classified as extremely arid (hyper-arid) punctuated by sudden catastrophic *torrents*.

Saint Anthony Cave developed within partially-dolomitic, sandy limestone (10%–20% quartz) of the Southern Galala Formation (Jochen Kuss, University of Bremen, personal communication, 2021), of late Paleocene-early Eocene age. This formation dips gently to the southeast and has highly fractured and weathered beds and calcite veins (Abdallah et al., 1970). This formation reaches a thickness of about 250 m (Scheibner et al., 2001) (Fig. 2).

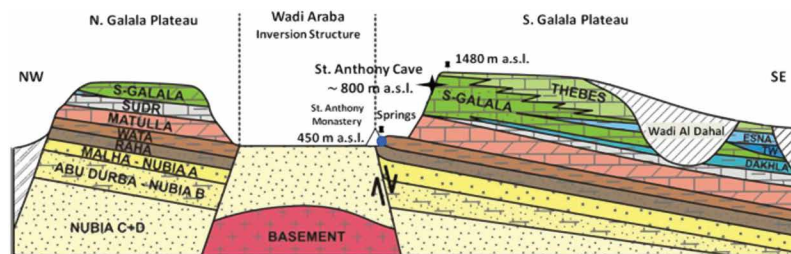


Figure 2. Geological cross-section of the North and South Galala Plateaus separated by Wadi Araba. Nubia C+D (sandstones), Nubia B (sandstones with shales/claystone, dolomites, and subordinate limestones), and Nubia A (sandstones occasionally shales/claystone) are Paleozoic to Early Cretaceous in age. The Raha, Wata, and Matulla Formations (a mixed facies sequence, containing marls, shales/claystone, sandstones, dolomites, and limestones) are Late Cretaceous in age. The uppermost Cretaceous rocks are represented by the Sudr Formation (chalk, chalky limestones). Paleocene and Eocene rocks are represented by S-Galala and Thebes Formations (sandy limestones, dolomitic limestones, limestones with marl intercalations, partly conglomeratic). Other formations in blue are marls and shales (Moustafa and Khalil, 2017; Moustafa and Khalil, 2020; Scheibner et al., 2001). The site of the cave is added according to the current study. The elevation points according to the GPS measurements and a topographic map at a scale of 1:50,000. The figure is adapted from Höntzsch et al. (2011).

SPRINGS

There are inactive and active springs and both hand dug and drilled wells in the study area, and most are located in Wadi Araba. Most of the springs are unconfined, but some are confined, and groundwater generally appears to be controlled by structural features (i.e., faults and folds), lithology, and topography (Aggour, 1990).

The water is brackish. Total dissolved solids range from 1.344 g L⁻¹ to 2.822 g L⁻¹, temperature ranges from 13 °C to 28.3 °C, and pH ranges from 6.9 to 8.5. The water type is mostly Cl (407–1,098 mg L⁻¹), SO₄ (200–848 mg L⁻¹), HCO₃ (129–405 mg L⁻¹), and isotopic measurements suggest meteoric recharge (Wannous et al., 2021; Khalil et al., 2021).

Four brackish springs emerge 340–354 m below Saint Anthony Cave in the Saint Anthony Monastery. They are (1) Saint Anthony, (2)

Maryam (Aladra), (3) Smar, and (4) Agathon Springs (Fig. 1C). The latter two springs have the highest SO_4 values recorded in the area. The Saint Anthony and Maryam Spring waters flow through active karst spring caves. They are fracture controlled and developed in upper Cretaceous carbonate rocks (Aggour, 1990). Currently, the springs below Saint Anthony Cave have low discharge volumes of about $5 \text{ m}^3 \text{ d}^{-1}$, except the spring of Saint Anthony has a constant discharge of about $100 \text{ m}^3 \text{ d}^{-1}$, which it has had since the 1st century AD, as documented by the monks.

The water chemistries of the springs of Saint Anthony and Maryam (Aladra) in February 2018 were brackish (1465 and 1547 mg L^{-1} dissolved salts, respectively) with a pH of 7.3 and 7.8, respectively. Their water types were Cl (407 and 437 mg L^{-1} , respectively)– SO_4 (314 and 349 mg L^{-1} , respectively)– HCO_3 (279 and 255 mg L^{-1} , respectively), and their temperatures were $24 \text{ }^\circ\text{C}$ and $17 \text{ }^\circ\text{C}$, respectively (Wannous et al., 2021). In January 2016, the water chemistry of the Saint Anthony spring was brackish (1335 mg L^{-1} dissolved salts) with a pH 7.3 and a water type of Cl (450 mg L^{-1}), HCO_3 (305 mg L^{-1}), SO_4 (180 mg L^{-1}) (Saint Anthony Monastery, unpublished data, 2016).

Based on the field investigation and the information from the monks, Saint Anthony Spring Cave (latitude $28^\circ 55' 22.98''$ N, longitude $32^\circ 21' 1.31''$ E) consists of a narrow entrance, less than 1 m wide and high. This entrance leads to a passage about 0.50 m wide, 0.80 m high, and 0.30 m depth below the water level that extends about 8 m to where the

water emerges from rocks (Fig. 3A). Maryam (Aladra) Spring Cave (latitude $28^\circ 55' 24.79''$ N, $32^\circ 21' 5.41''$ E) consists of an entrance room that measures about $4 \text{ m} \times 3 \text{ m}$, with a height of about 3 m above the water level and a depth of about 1 m below the water level. This room connects upstream to a narrow passage about 1 m wide (Fig. 3B).

Our personal observations show that the Saint Anthony spring cave has a corrosion table slightly higher than the water level of the spring. The Maryam (Aladra) Spring Cave shows corrosion tables, nearly flat ceiling pendants, a small



Figure 3. Active karst spring caves, Saint Anthony (A) and Maryam (Aladra) (B), at the Saint Anthony Monastery.

smooth curving channel on the wall, with likely secondary gypsum. These features are common in sulfuric acid caves (e.g., Audra et al., 2009) and suggest that sulfuric acid may have been involved in the formation of Saint Anthony and Maryam Spring Caves.

REGIONAL TECTONIC HISTORY AND AREA BACKGROUND

Late Cretaceous to early Paleocene pulses of tectonic deformation across the study area produced the asymmetrical plunging anticline of Wadi Araba with nearly vertical beds at the Saint Anthony Monastery (Moustafa and Khalil, 1995). There is a debate about whether or not Wadi Araba is the expression of a fault-propagation fold (Moustafa, 2020) with a deep-rooted fault present at the northern cliff of the Southern Galala Plateau that separates Wadi Araba from the plateau (Schütz, 1994). From the late Paleocene to the middle Eocene, the area was under marine conditions (Said, 1962), and the upper Paleocene/lower Eocene rocks in which Saint Anthony Cave has formed were deposited.

There are no deposits dating from the late Eocene until the Miocene present in the Southern Galala Plateau and until the Pleistocene present in Wadi Araba (e.g., Klitzsch et al., 1987). However, sediments dating from these periods were recorded at the eastern side of the Gulf of Suez Rift directly opposite the study area. There, late Eocene marine deposits are recorded by the shallow marine Tanka Formation (Hume et al., 1920; Abul-Nasr and Thunell, 1987). The deposition of the Tanka Formation in the study area is a matter of debate; most workers have suggested that it was deposited and later eroded. In the middle Oligocene, a global major eustatic sea level drop occurred (Haq, 1987). The study area was exposed to erosion before the Gulf of Suez Rift was initiated, and the erosion was not more than a few hundred meters (Garfunkel, 1988).

From possibly the middle Oligocene or late Oligocene to the early Miocene, the Gulf of Suez Rift began to open at sea level (e.g., Robson, 1971; Garfunkel and Bartov, 1977; Patton et al., 1994; Bosworth and McClay, 2001; Moustafa and Khalil, 2020). Continental conditions are recorded in the first syn-rift formation called “Abu Zenima” (Hantar, 1965), which was deposited under arid and semi-arid climate conditions (Jackson et al., 2006). Volcanic activity that preceded the rift phase was recorded and assigned a variety of ages. The oldest exposed late Cenozoic volcanic basaltic dike in the Gulf of Suez area has been dated at $25.7 \pm 1.7 \text{ Ma}$ in the Southern Gabel Ataqa (Bosworth and McClay, 2001), north of the study area.

Non-marine conditions were followed by shallow marine conditions at the 2nd syn-rift formation called “Nukhul” (Egyptian General Petroleum Corporation, 1964). The Nukhul Formation recorded slow subsidence rates of the rift and

it is early Miocene (Aquitanian-early Burdigalian or early Burdigalian) in age (e.g., Evans, 1990; Bosworth and McClay, 2001).

The margins of the Gulf of Suez Rift and the plateau have been uplifted, but the timing of the uplift is unclear. Omar et al. (1989) used apatite fission track analysis on the rocks of the western margin of the Gulf of Suez rift and concluded that the beginning of uplift in the area was at 22 ± 1 Ma.

In the early Miocene (Burdigalian), uplift of the margins of the Gulf of Suez Rift accelerated and was accompanied by subsidence of the Gulf of Suez Rift. This persisted until about 17 Ma (mid-Clysmic event); then the uplift and subsidence decelerated (Garfunkel and Bartov, 1977; Moretti and Colletta, 1987; Steckler et al., 1988; Evans, 1988; Richardson and Arthur, 1988; Jarrige et al., 1990; Patton et al., 1994; Bosworth and McClay, 2001; Moustafa and Khalil, 2020). Open and deep-marine conditions were recorded in the central parts of the Gulf of Suez Rift Basin during deposition of the *Burdigalian-middle Langhian* Rudeis Formation (Egyptian General Petroleum Corporation, 1964). In the Southern Galala Plateau, the syn-rift formations are recorded at the eastern margin of the plateau and unconformably overlay the middle Eocene rocks (Egyptian Mineral Resources Authority, 2005).

METHODS

Although Saint Anthony Cave is relatively small, large numbers of visitors made it difficult to conduct detailed fieldwork in one day. Different one-day trips were carried out from August 2015 to August 2021. The fieldwork was performed using measurements, observation, and information from monks living in the monastery. We surveyed the cave in detail on June 15 and August 3, 2021, using a compass and clinometer with 0.5° of accuracy, a laser range finder, and tape.

Because the cave opening is in a steep scarp face, approximate coordinates and altitude of the cave were determined based on the GPS measurements integrated with a 1:50,000-scale topographic map. Cave minerals were identified in the field based on observations and on the use of hydrochloric acid.

Cave mapping was conducted using the methods outlined in Chabert and Watson (1981) and Dasher (1994). Cave survey data processing was performed using ArcGIS 10.3. Cave symbols used in the cave map are based on National Speleological Society standard map symbols by Hedges et al. (1979), as well as the caves style symbols in ArcMap, and suggested symbols.

RESULTS

Cave Morphology

Saint Anthony Cave consists of an upper-level passage, 4.43 m^2 , leading to a lower-level room, 17.70 m^2 . The cave has a total area of 22.13 m^2 , volume of 44 m^3 , length of 17.10 m , and depth of 5.33 m . The cave entrance is a horizontal, fracture-controlled opening. It is $2.22\text{--}2.70 \text{ m}$ high and $0.68\text{--}1.25 \text{ m}$ wide (Figs. 4, 5(A)). The cave entrance was very narrow but has been artificially widened by the monks of the monastery.

Immediately outside the cave entrance, the floor takes the shape of the conduit and extends outward for 5.20 m . The sides of this conduit-like passage are the side faces of a deep notch. Small, relict speleothem deposits are present on

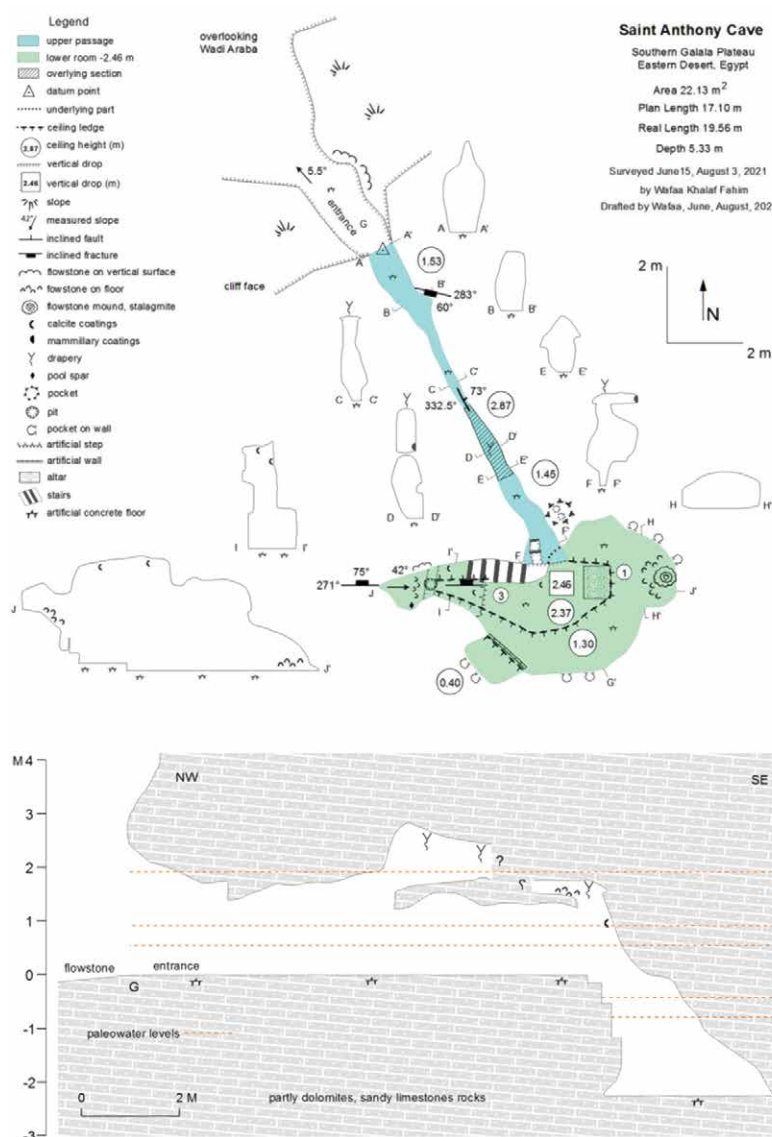


Figure 4. Map of Saint Anthony Cave showing a plan view, cross sections, and longitudinal profile. The yellow section is the entrance passage, and the green section is the terminal room. (The floor steps are artificial.)

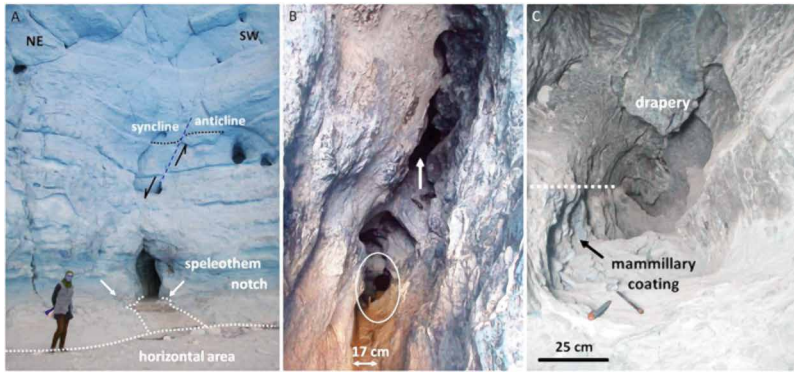


Figure 5. (A) Front view of the entrance of Saint Anthony Cave in the year 2015 showing speleothems (*white arrows*), a normal fault (*dashed red line*), and faces of a notch (*dashed white lines*). (B) Cave passage illuminated by morning daylight (looking inward) showing a person for scale (*white circle*), a vertical metal stair railing (*white, west of the person*), and the overlying section shown in Fig. 5C (*white arrow*). (C) Overlying sub-horizontal section showing a paleowater level (*dashed white line*).

parallel fracture occurred during the opening of the Gulf of Suez Rift at Oligocene-Miocene time (Moustafa and Khalil, 2020).

The entrance passage is nearly straight, steeply inclined at the start, and very narrow with irregular cross sections (Fig. 5B). The passage ranges from 0.17 to 1.00 m wide and from 1.35 to 2.87 m high. The passage varies in height along its entire length. The width of the passage also varies inversely with passage height, i.e., the narrow parts are higher and the wide parts are lower.

The cave passage ends at the terminal room. Near the junction between the entrance passage and the terminal room, the main fracture along the passage gradually changes orientation to another steeply-inclined fracture oriented N 89° W (271°) that dips to the north at 75° and that runs along the western side of the room. It is not clear whether this fracture is a fault or a joint, but the trend of this fracture is similar to the orientation of the transverse or cross faults (N 50°–75° E). The transverse faults were active during the opening of the Gulf of Suez Rift and developed through the reactivation of pre-existing basement fractures (Patton et al., 1994; Moustafa and Khalil, 2020). The passage drops 2.46 m into the terminal room. The terminal room is 7.76 m long and ranges from less than 1 m to 4 m wide and from less than 1 m to 3 m high with irregular cross sections.

Meso- and Micromorphological Features

The most significant feature of Saint Anthony Cave is an upward branch of the upper-level entrance passage. This branch has formed along the same fracture as the main passage and is associated with the highest and narrowest part of it. This overlying section is 0.50 m wide and penetrates 2.10 m sub-horizontally toward the inner parts of the cave and apparently ends just out of sight. Inside this feature, there are niche-like features (convection-related features) are at the same level, but their origin is not clear (Fig. 5C). This overlying section may be a small sub-horizontal passage or a modified fracture-controlled chimney, and it may represent the early or the later dissolutional phase of the cave development.

Almost all the features of the floor of the cave are obscured by concrete and in some places the lower parts of the cave wall as well. There are other structures that have been built in the terminal room, obscuring some of the natural features. But 0.90 m before the inner termination of the passage, it contains a fissure in its floor. Along this downward-narrowing floor, there are three small stairs with a total vertical drop of 1.30 m connected to the stair of the terminal room. According to the monks of the monastery, these steps are artificial and overlie a deep floor fissure both there and at the middle section of the passage, but they sealed the fissure to protect the visitors (Fr. Ruwais Al Antony and Fr. Faltaos Al Antony, personal communications). The floor of the terminal room is flat, except the westernmost side. There, a sloped floor has terraces that cut into thick layers of flowstone. Other dissolution or precipitation features in the floor of the cave are unknown.

A cupola-like feature and a ceiling-bell hole are found at the junction between the upper-level entrance passage and the lower-level terminal room. Both of these features have formed near each other at slightly different levels (Fig. 6A–E). The cupola-like feature has formed along the entrance passage fracture. This feature is 0.60 m long, 0.40 m wide, and 0.25 m high. It is undermined and some parts of it are not directly observable. The cupola-like feature is decorated by mammillary coating, draperies, flowstone, and one small stalagmite on its floor. It is not clear whether the cupola-like feature dead-ends or connects to the overlying branch of the entrance passage.

the sides of the notch.

The cave entrance leads to a passage 9.35 m long (from the datum of the cave). This cave passage is controlled by a steeply-inclined fracture oriented 332.5° that dips northeast at 73°. There is no definite evidence that this fracture is a fault or a joint, but there is a steeply-inclined, normal fault through the heavily-weathered cliff face immediately above the cave entrance. This fault has about 10 cm displacement and has a dip and a strike similar to the fracture along the entrance passage.

The extension (if present) of this fault downward is not clear, but it may be the fracture that appears at the eastern side of the cave entrance. It is likely that the cave passage is fault controlled, at least in the higher, middle parts of it. The trend of the fracture of the cave passage is called “clysmic” or “rift parallel.” The rift-par-

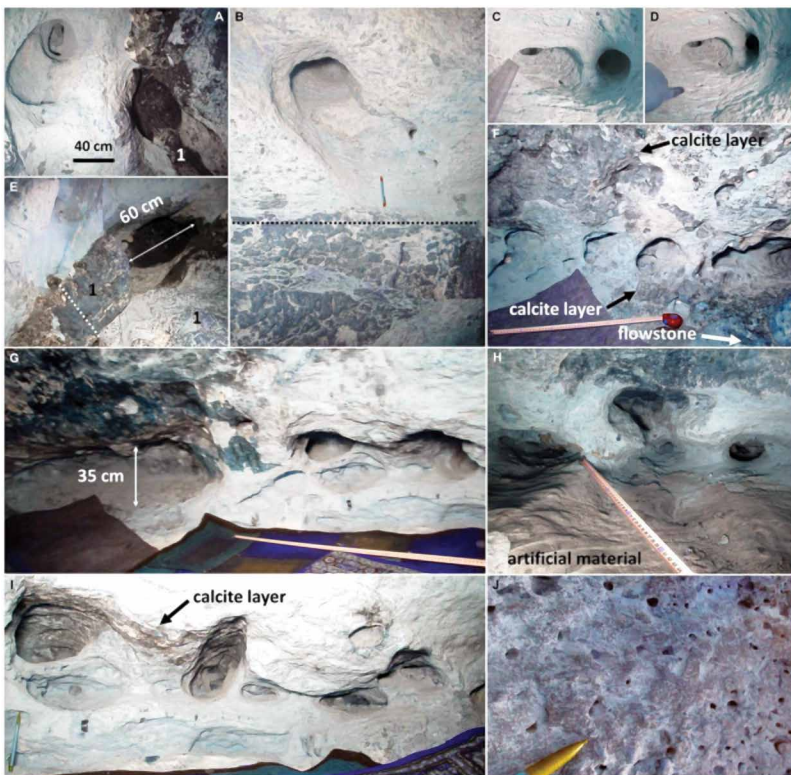


Figure 6. (A–E) Cupola-like feature and bell holes on the ceiling at the junction of the entrance passage and the terminal room. Figs. 6C and 6D are located inside the opening shown in Fig. 6B. In Figs. 6A and 6E, the numeral 1 refers to a thick calcite layer. In Figures 6B and 6E, the dashed lines show paleowater levels. (F–I) A series of dissolution pockets in the lower part of the southern wall of the terminal room. Fig. 6F is located at the northeast side of the terminal room. Fig. 6I is a close up view of the pocks in Fig. 6G. (J) Small hollows in the upper part of the wall of the passage.

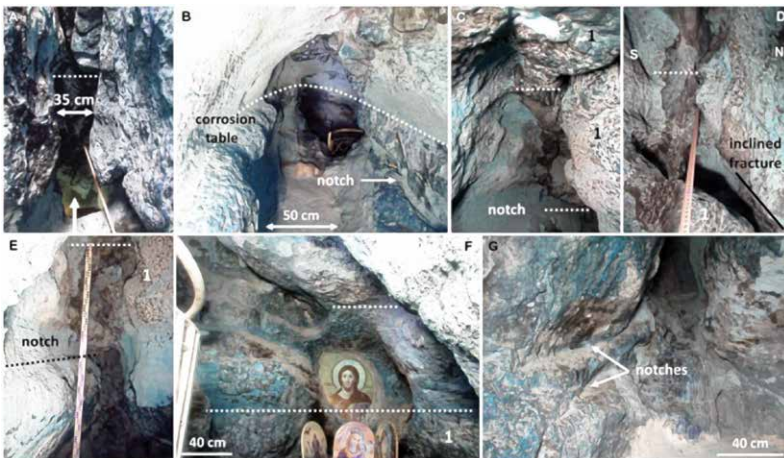


Figure 7. Paleowater levels (dashed lines). (A) Ceiling of the passage (white arrow points to the overlying section). (B) Back part of the entrance passage. (C) Upper part of the western side of the terminal room. (D) Ceiling of the westernmost side of the terminal room, looking upward. (E) Western side of the terminal room. (F) Hanging wall of the eastern side of the terminal room. (G) Lower part of the southwest side of the terminal room. The numeral 1 refers to a thick calcite layer with white weathering rinds.

The ceiling bell hole is formed along a minor, mineral-filled fracture above a paleowater level and reaches 0.90 m in height and 0.55 m in diameter. This feature branches inside into 2 small cylindrical holes, and one of them does not connect directly to the main hole. No deposits have been observed inside it.

Dissolution pockets are found in the cave's ceiling and walls. The wall dissolution pockets are concentrated in the lower parts of the southern and eastern sides of the terminal room. Some of them have formed along bedding planes. Others do not follow visible fractures and sometimes have a spongework texture or resemble replacement pockets (sulfuric acid-related pockets, usually small with a smooth inner surface, with replacement gypsum). They have no noticeable gypsum crusts. The bedding plane-controlled pockets are limited to the southern side of the terminal room. These are not connected, blind, and do not exceed 1 m deep. A few of them are connected to the floor of the terminal room and show very shallow channels on the floor. Small hollows with various shapes and sizes have also been observed throughout the cave (Fig. 6F–J). Remnants of wall pockets have also been found (Fig. 7F).

Former water level positions are present in the cave. There is a definite correlation between the elevation of one paleowater level inside the cave and a notch in the cliff face outside the cave. The relationships with other paleowater levels are difficult to examine. The paleowater levels can be seen as poorly developed notches, corrosion tables, paleowater lines, and flat ceilings (Fig. 7A–G). The paleowater levels were measured relative to a single datum located at the middle part of the entrance passage using a laser range finder.

In the entrance passage, 3 major paleowater levels are present at 2.10 m, 0.95 m, and 0.60 m above the datum. In the terminal room, there are 3 notable major paleowater levels. The 1st level at 0.55 m above the datum approximately corresponds to the 3rd paleowater level in the entrance passage. The other major levels are located in the terminal room at 0.45 m and 0.85 m below the datum. Very shallow notches have also been found in 2 lower parts of the wall of the terminal room.

Speleothems

Speleothems are secondary mineral deposits in caves. Saint Anthony Cave is currently moderately decorated with inactive speleothems, and most bedrock fractures have filled with minerals. Most of the speleothems are decomposed. Some are partially eroded, or visible only as remnant patches (Fig. 8A–B). Others have small

erately decorated with inactive speleothems, and most bedrock fractures have filled with minerals. Most of the speleothems are decomposed. Some are partially eroded, or visible only as remnant patches (Fig. 8A–B). Others have small

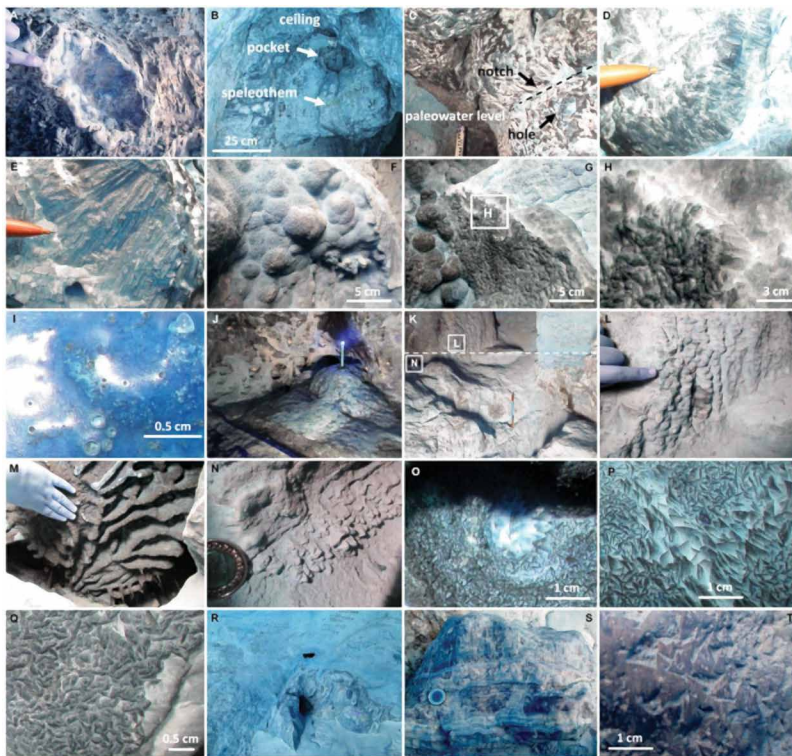


Figure 8. (A) Remnant of speleothem on the wall of the passage near the cave entrance. (B) Block of speleothem in the ceiling near the cave entrance. (C) Thick calcite layer on the wall of the northern side of the terminal room. (D) Internal structure of the thick calcite layer in the terminal room. (E) Columnar calcite crystals in a hanging wall in the terminal room, looking upward. (F) Mammillary coating in the overlying section of the entrance passage. (G) Mammillary coating at the cupola-like feature. (H) Close up view of the internal structure of the mammillary coating in Fig. 8G. (I) Thin flowstone with pits in the terminal room. (J) Flowstone on the floor at the easternmost side of the terminal room. (K) Waterfall flowstone at the westernmost side of the terminal room, showing a paleowater level (*dashed line*) and the location of Figs. 8L and 8N (*white boxes*). (L) Subaqueously-formed popcorn on the surface of the flowstone. (M) Draperies on the ceiling of the cupola-like feature. The black color is a fire-smoke pigment. (N) Pool spar. (O and P) Calcite crystals in the cupola-like feature. (Q) Modified crystals with vermicular texture on the surface of a speleothem in the cave passage. (R) Relict speleothem on the face of the notch outside the cave on the eastern side of the cave entrance. (S) Cross section of the speleothem that is shown in Fig. 8R looking downward. Coin is 2.5 cm in diameter. (T) Triangles of calcite crystals on the surface of the speleothem in Figs. 8R and 8S.

modified macro crystals, giving the surface a vermicular texture (Fig. 8Q).

A thin layer of calcite has been found in the lower parts of the eastern side of the terminal room. This layer has covered the low ceiling and parts of the wall, and it has lined most of the dissolution pockets (Fig. 6F–I).

Outside the current cave entrance, speleothems have only been found in two areas as flowstone deposits. The first deposit is located 1.35 m away from the cave entrance and east of it. It is present on the face of the notch and has covered an area of 1.5 m². A cross section of a part of this speleothem shows alternating, slightly wavy bands of whitish, creamy, and brownish calcite, totaling 21 cm. The surface is usually macrocrystalline and shows triangular crystals that are dark brown (Fig. 8R–T).

The 2nd flowstone deposit is located 1.5 m east of the first deposit. This speleothem lines an enlarged small fracture that dissects the floor of the notch. This deposit has colored-banded layers similar to the first deposit. Apparently, those speleothems were formed in an enlarged fracture and cavity and then were intersected by the later erosion (the notch) although they could be misinterpreted as having been deposited on the notch floor.

In 2015, there were speleothems on the western side of the cave entrance as well, but they were removed by human modification. No other speleothems have been found outside the cave.

DISCUSSION

holes or are coated by thin, white, weathering rinds composed of fine-grained calcite.

The speleothems in the cave are layers of calcite, mammillary coatings, flowstone, draperies, spar, and a few small stalactites. Nearly all speleothems are composed of calcite, sometimes with impurities.

The most notable speleothem in the cave is a thick layer of calcite in the upper and middle parts of the terminal room. The surface of this layer is very weathered and displays holes and white rinds. The surface is coarsely crystalline with distinct crystal faces, while its internal structure shows columnar crystals up to 6 cm in length (Fig. 8C–E).

Mammillary coatings have been observed in the overlying section of the entrance passage and in the inner wall of the cupola-like feature. The latter coating has columnar crystals a few centimeters thick and all the mammillaries have modified macrocrystalline surfaces (Figs. 5C, 8F–H).

The flowstone ranges from less than 1 mm to several centimeters thick. It can be clearly seen in the terminal room on the wall, on the terraced floor, and in the easternmost side as a sheet and small, stalagmite-like deposits. Some flowstone that is associated with the paleowater levels shows an irregular, crenulated surface with subaqueous calcite coralloids (Fig. 8I–L). The draperies are found in localized areas along the ceiling fractures and in the cupola-like feature (Fig. 8M). A few terminate with stalactites.

Spar lines a small pool at the western side of the terminal room and is adjacent to subaqueous popcorn. The spar is one centimeter or less in size (Fig. 8N). Macro crystals are also observed in the cave. They can be seen on the ceiling of the cupola-like feature and on the draperies inside, and they are adjacent to the mammillary coating (Fig. 8O–P). Some speleothems display

This study complements previous work and interpretation of the speleogenesis of Saint Anthony Cave as primarily phreatic. Our new results support that origin with new observations of paleowater-level dissolution features and at least four phases of cave development. The volcanic and tectonic background of the area suggests a high possibility of the contribution of deep fluids in the formation of the cave, supporting a hypogene origin (e.g., Klimchouk, 2007; Klimchouk, 2009; Palmer, 2007), at least in the earliest phase of development.

At a regional scale, Saint Anthony Cave is located within a cliff face adjacent to a deep-rooted fault and the steeply-inclined flank of an asymmetrical anticline. The bedrock containing the cave has been subject to extensional tectonics owing to its proximity to the western margin of the intracontinental Gulf of Suez Rift. Late Oligocene volcanic bodies are present in the vicinity of the cave (Fig. 1A–C). These settings and environments have been shown to be conducive to hypogene speleogenesis (Klimchouk, 2017).

There is no strong speleogenetic relationship between the cave and overlying or adjacent surface features. The strata overlying the cave are thick and mainly carbonates. The surface of the plateau directly above the cave (about 100 m above the cave entrance) has a hanging, dry, and small catchment area with autogenic recharge. Surface water flows from this catchment area in the direction of Wadi Araba, opposite the downward-gradient direction of the cave. Sinkholes, sinking streams, and shafts are absent. Floodwater-cave characteristics are not distinct (e.g., small waterfalls, few speleothems) (Palmer, 2007). Backflooding from Wadi Araba cannot be ruled out, but it did not initiate the speleogenesis, as discussed below.

Saint Anthony Cave is controlled by steeply-inclined fractures that are probably faults. The cave floor rises in the downstream direction of the cave. The cave varies in size and morphology with irregular cross-sections. The cave ends abruptly along fractures and bedding planes with blind terminations. Dissolution pockets, cupola-like features, ceiling bell holes, notches, corrosion tables, and flat ceilings are present in the cave. The floor of the entrance passage, in some parts, was originally a fissure extending downward, likely a feeder that transmitted water from depth and later partially choked by calcite deposits. This fissure has now been mostly filled and covered in concrete.

Remnants of the speleothems everywhere in the cave, especially at the cave entrance and immediately outside the cave, indicate that the cave extended beyond the current threshold. It was very decorated and opened after depositional conditions by cliff retreat. Paleowater level features superimposed on the subaerial speleothems suggest inundation following subaerial deposition.

The thick calcite layer is absent from the later-enlarged parts, and where it is present, it has been partially dissolved along distinct horizons. The interior columnar structure of this layer is similar to those in the mammillary coating found in the cupola-like feature. Additionally, nearly all the white-weathering rinds in the cave have been found on its surface except a few occurrences on bedrock walls.

White rinds form by dissolution in the presence of moisture and cave air rich in carbon dioxide, and this process is more effective if the cave air contains hydrogen sulfide (Palmer, 2007). It is clear the thick calcite layer is a relic of the earliest phase of the cave development. This calcite layer was likely deposited subaqueously and was modified by later events.

The depositional age of the well-defined mammillary coatings is difficult to determine. They may have formed early in the early cave's development and were preserved because of their protected positions or formed during a later phase of the cave development.

The depositional environment of the thin calcite layer located in the lower part of the eastern side of the terminal room is not clear. This layer has a coarse texture similar to a wall calcite layer located above the pool spar. This layer was likely deposited during later subaqueous conditions. Further work could be done to establish the age and depositional environment of the calcite.

The speleothems located immediately outside the cave show characteristics of the Egyptian calcite-alabaster as documented by Halliday (2003). Egyptian calcite-alabaster consists of thin straight to curved bands of creamy-white opaque calcite crystals alternating with thicker layers of brownish, translucent calcite crystals (Harrell et al., 2007). Egyptian alabaster has been observed in some caves in the northern cliff of the Southern Galala Plateau. These deposits are also known in the Northern and Southern Galala Plateaus (Abu Zeid and Mazhar, 1992). An isotopic study by Tourre (2000) estimated water temperature between 32 °C and 86 °C for the Egyptian calcite-alabaster from an ancient quarry in Wadi Araba and attributed it to the hydrothermal solution (Harrell et al., 2007). The triangular crystals on the surface of these deposits are parallel to the growth surface and probably formed later under subaqueous conditions.

Scalenohedral calcite crystals common to thermal deposits (Dublyansky, 2013) were observed inside the fracture outside the cave. These crystals are also present in the cave, but there is no direct evidence of their origin. Within the cave, smooth bedrock walls, ceiling bell holes, and niche-like features are located just above the paleowater levels. These features may indicate condensation-corrosion processes by convective airflow above thermal/warm water (e.g., Cigna and Forti, 1986; Audra et al., 2009).

Currently, the springs below the cave and in Wadi Araba have been classified as cold (e.g., Khalil et al., 2021;

Wannous et al., 2021), although the data of the latter study show a few springs with water temperatures 4 °C to 5 °C higher than the average annual air temperature in the area (23.36° C). Those latter few springs are considered slightly thermal or warm according to the 4 °C threshold of Schoeller (1962). Thermal springs are known in the surroundings of the Northern and Southern Galala Plateaus (Fig. 1A–C). The thermal paleowater was present in the past and likely contributed to the development of the cave.

No gypsum or anhydrite rocks are known in the northern side of the Southern Galala Plateau. No secondary gypsum has been observed inside Saint Anthony Cave although it may have been removed by later processes. Two springs below the cave have the highest sulfate values in the area. Features that suggest sulfuric acid speleogenesis (e.g., Audra et al., 2009), such as flat ceilings, corrosion tables, notches, pockets with spongework texture, and replacement-like pockets, are present in Saint Anthony Cave. While the remaining evidence is inconclusive, dissolution by sulfuric acid cannot be ruled out.

Wadi Araba and the Cave Evolution

Saint Anthony Cave overlooks Wadi Araba and is located at its eastern margin. The cave entrance opened by the retreat of the northern cliff of the plateau during the incision and widening of the wadi. The timing and the processes that formed the wadi may provide additional clues for the age and the speleogenetic phases of Saint Anthony Cave, as described below.

Wadi Araba extends from the west-southwest to the east-northeast for about 85 km with an area of about 2000 km². The wadi is characterized by the presence of residual hills, shallow channels, and large paleo-alluvial fans left by the smaller wadis that drained into it.

The Wadi Araba anticline has undergone erosion, exposing Carboniferous rock in the anticline core that has become overturned. It extends offshore into the Gulf of Suez Rift basin. Paleocene and Eocene rocks are absent in the offshore extension of the anticline (Moustafa and Khalil, 1995). Schütz (1994) assumed Miocene surface karst erosion of the Eocene units. In the basin adjacent to this extension, thick sands derived from the rocks of the Wadi Araba anticline are recorded in the Rudeis and Kareem Formations (post-Aquitania) (Schütz, 1994).

Additionally, the sand isolith maps of the syn-rift formations at the *offshore extension* of the *Wadi Araba* anticline show a negligible volume of sands in the 2nd syn-rift Nukhul Formation and a large volume in the Rudeis and Kareem Formations (Peijs et al., 2012). These sands were derived from the erosion of the Wadi Araba anticline (Moustafa and Khalil, 2017). These studies suggest the strong erosion phase of the Wadi Araba anticline was post-Aquitania, particularly in Burdigalian and Langhian times.

The youngest formation that is recorded in the highest altitude areas of the Southern Galala Plateau formed in the middle Eocene. Currently, the cave is located at about 800 m MSL. The maximum altitude of the plateau is 1480 m MSL and is covered by the middle Eocene rocks. Therefore, the rock hosting the cave was at least 680 m or more below the surface prior to the opening of the Gulf of Suez Rift.

Saint Anthony Cave has phreatic characteristics and was controlled by fractures having orientations similar to the rift-related fracture trends. The cliff face at the cave is dissected by normal faults dipping towards the Gulf of Suez Rift. The coincidence of these trends suggests it is likely that the cave fractures were related to rifting.

The timing of the primary erosion phase of the Wadi Araba anticline is synchronous with rapid uplift in Burdigalian time (e.g., Moustafa and Khalil, 2017). Uplift and valley incision would have likely lowered the water table. These were followed by an abrupt drop in global sea level in the late Miocene followed by sea level rise in the early Pliocene (Haq, 1987). The later immersion of the cave probably occurred post-Miocene. Therefore, the phreatic phase of the cave is no younger than Burdigalian or probably no older than the beginning of the opening of the Gulf of Suez Rift in Chattian time. We propose that the speleogenesis initiated with the onset of the rifting.

In the late Oligocene (early Chattian), the Gulf of Suez Rift began to open. Volcanism preceded the rifting and is recorded proximal to the study area by basaltic dikes, sills, and lava flows at the base of the syn-rift succession (e.g., Steen, 1984; Meneisy, 1990). A large dike of age 22.3 ± 0.2 Ma is also present 3 km west of the Saint Anthony Monastery at approximately 553 m MSL (Bosworth et al., 2015) (Fig. 1C).

Volcanism affected the chemical and thermal attributes of the groundwater and would have increased heat flux during that time, increasing groundwater temperature and also the CO₂ and H₂S content of the water (Klimchouk, 2017).

Extensional tectonics would have likely enhanced the upwelling of deep fluids (e.g., Sibson, 1996). The large anticline of Wadi Araba, the deep-rooted fault of the wadi, and related fractures would provide favorable flow paths for ascending deep groundwater.

Both CO₂ and H₂S are commonly present together in deep groundwater (Klimchouk, 2019). Accordingly, the speleogenesis began in the presence of CO₂/H₂S and thermal water. More than one dissolution mechanism could have operated either sequentially or simultaneously, such as CO₂/H₂S, cooling thermal water, mixing of high-CO₂ thermal water with low-CO₂ shallow water, and mixing of water of contrasting chemistry.

Saint Anthony Cave and other caves began to form, particularly in the area surrounding the deep-rooted fault. Dis-

solution would have also been concentrated within the carbonate rocks along the crest of the Wadi Araba anticline.

Until the earliest Burdigalian, there was little uplift of the rift shoulder (e.g., Garfunkel and Bartov, 1977; Bosworth and McClay, 2001; Moustafa and Khalil, 2020). In Burdigalian time the uplift rates of the rift shoulder increased, uplifting the study area to shallower hydrologic conditions. Under these conditions, dissolved CO₂ forms a separate phase, and calcite precipitation can occur (Dublyansky, 2013). The solutions eventually favored subaqueous calcite deposition. Then the cave was uplifted into a vadose setting (Table 1).

In the late Miocene (about 7.5 Ma), humid climatic conditions were prevalent in the Gulf of Suez Rift and the Red Sea

Table 1. The main phases of the development of the Saint Anthony Cave.

Phase	Time	Condition	Main Process
1	Possibly middle Oligocene to early Miocene (Burdigalian) (about 17 MYA)	Volcanism, extensional tectonic activity, deep-seated acids, deep-rooted fractures, thermal water	Dissolution and precipitation
2	Late Miocene (about 7.5 Ma)	Base level fall, humid climate conditions	Precipitation
3	Post-Miocene or early Pliocene	Base level rise	Dissolution and precipitation
4	Post-Miocene	Base level fall	Precipitation

areas (Griffin, 2002) with a *large drop in global sea level* in the Messinian time. During this time, the cave was characterized by the growth of subaerial speleothems.

Post-Miocene, particularly in the early Pliocene, global sea level rose (Haq, 1987) and reached up to 200 m MSL in combination with continued extensional tectonic activity in the southern part of the Gulf of Suez Rift area (Bosworth and McClay, 2001). The rising sea levels elevated the base level, and the cave was submerged. During upwelling/lowering the water level, dissolution processes occurred at and above the water level. During this 3rd phase, infiltrating meteoric water very likely was involved, and more than one dissolution mechanism was occurring. Back-flooding from Wadi Araba likely has also been involved.

This 3rd speleogenetic phase can clearly be seen in the paleowater levels features superimposed on the speleothems of previous phases (Fig. 7), although the notches in the cave could have formed from water oscillations. Other features such as the corrosion table, flat ceiling, pockets with spongework texture, and replacement-like pockets may reflect sulfuric acid dissolution during this phase.

The branching bell hole is located above a paleowater level at a later-enlarged part of the cave. These bell holes did not have speleothems, likely because they have formed along a mineral vein, supporting a later phase for their origin. The origin of dissolution niches is not clear, but they resemble convection niches features that form above the surface of thermal/warm ponds (Audra et al., 2009). There are well-preserved crystals, likely scalenohedral calcite crystals in the cupola-like feature and in the small pool. All these features may indicate that there was thermal/warm water in the cave during the 3rd phase.

The correlation between one paleowater level inside the cave, with a notch outside the cave, with and the absence of speleothems on the floor of the notch outside the cave, suggest that the cave was exposed to the surface at or slightly after the 3rd phase. This likely occurred during the latter filling phase of Wadi Araba. The cave appears to be a fossil overflow route as suggested by Halliday (2001) and was an active spring with likely sulfuric thermal/warm water.

When the water levels lowered, the cave dried out and was again characterized by speleothem deposition under wetter climatic conditions of later periods.

More than one dissolution mechanism such as mixing dissolution has likely been involved in the formation of the cave and the area in general. Dissolution was prominent in Oligocene-early Miocene time when volcanic activity was followed by extensional tectonics that provided deep fluids and deep-rooted fractures, and when the uplift rates of the area were slow. It is most likely that there are other caves near Saint Anthony Cave and in the area that have not yet opened to the surface.

CONCLUSION

A detailed map has been created of Saint Anthony Cave. The cave opens within the northern cliff face of the uplifted Southern Galala Plateau at about 800 m MSL. The cave is a steeply-inclined, fracture-controlled, isolated cave consisting of a very narrow entrance passage ending in a small, lower-level, terminal room. A small overlying section is present in the entrance passage. The cave has an irregular profile and cross sections and has characteristics of phreatic and water table caves. The cave has little relationship to the surface features and has opened by scarp retreat. This study identified four phases of cave development caused by different processes at different times:

1. An early phreatic phase, before uplifting (late Oligocene to early Miocene), when volcanic and tectonic activities

- fractured the rocks and provided deep acids and heat, enhancing dissolution by different mechanisms;
2. A speleothem depositional phase, after uplifting (late Miocene, about 7.5 Ma) during humid conditions;
 3. A dissolution and depositional phase (early Pliocene/post-Miocene), when the base-level rose, flooding and enlarging the cave at and above the water level, and when sulfuric thermal/warm water likely was present; and
 4. A speleothem depositional phase (post-Miocene) during humid climatic conditions of later periods.

Presently, Saint Anthony Cave is inactive and is exposed to dissolution by acidic moisture. Recent corrosion may be due to carbon dioxide emissions from candle smoke and other human activity. Therefore, we highly recommend replacing the candles with a clean light to preserve this important religious, cultural, and historic cave. We expect this research to be helpful for more advanced studies, such as isotopic analysis of the speleothems.

ACKNOWLEDGEMENTS

We gratefully acknowledge Professor Adel Ramadan Moustafa (Faculty of Science, Ain Shams University) and Professor John Mylroie (Mississippi State University) for helping us to carry out this study. We thank Professor Mylroie for the constructive review of the manuscript more than once, for his encouragement, and for other support. We thank Professor Ramadan for the constructive review of the regional tectonic history section, for correcting a misunderstanding about the geological structure of the area, and for all other support. We thank Professor Ashraf Roshdy Baghdadi (Faculty of Science, Ain Shams University) for helpful discussions about sedimentary rocks. We thank the monks Fiar Ruwais Al Antony and Friar Faltaos Al Antony and the workers of Saint Anthony Monastery for their help during this research work. We thank as well Professor Jochen Kuss (University of Bremen) for helping us to identify the lithology and the age of the cave rocks. We thank Associate Editor Paul Burger for improving the language of the article and for constructive comments. Comments by anonymous reviewers helped improve the manuscript.

REFERENCES

- Abdallah, A.M., El Sharkawi, M.A., and Marzouk, A., 1970, Geology of Mersa Thelmet area, Southern Galala, Eastern Desert, A.R.E.: Bulletin of the Faculty of Science Cairo University, no. 44, p. 271–280.
- Abul-Nasr, R.A., and Thunell, R.C., 1987, Eocene eustatic sea level changes: Evidence from western Sinai, Egypt: *Palaeogeography, Palaeoclimatology, Palaeoecology*, v. 58, p. 1–9, [https://doi.org/10.1016/0031-0182\(87\)90002-2](https://doi.org/10.1016/0031-0182(87)90002-2).
- Abu Zeid, K.A., and Mazhar, A., 1992, Stratigraphical Geology of the Galalas and Wadi Araba, North Eastern Desert, Egypt: Egyptian Geological Survey and Mining Projects Authority, Reports 6/89 and 13/90, 20 p.
- Aggour, T.A., 1990, Response of geomorphological and geological features on groundwater in Wadi Araba, Eastern Desert, Egypt [M.S. thesis]: Ain Shams University, 237 p.
- Audra, P., Mocochain, L., Bigot, J.-Y., and Nobécourt, J.-C., 2009, Morphological indicators of speleogenesis: Hypogenic speleogens, in Klimchouk, A.B. and Ford, D.C., eds., *Hypogene Speleogenesis and Karst Hydrogeology of Artesian Basins: Simferopol, Ukraine, Ukrainian Institute of Speleology and Karstology*, special paper 1, p. 23–32.
- Bosworth, W., and McClay, K., 2001, Structural and stratigraphic evolution of the Gulf of Suez Rift, Egypt: A synthesis, in Ziegler, P.A., Cavazza, W., Robertson, A.H.F., and Crasquin-Soleau, S., eds., *Peri-Tethys Memoir 6: Peri-Tethyan Rift/Wrench Basins and Passive Margins: Paris, Mémoires du Muséum National d'Histoire Naturelle*, v. 186, p. 567–606.
- Bosworth, W., Stockli, D.F., and Helgeson, D.E., 2015, Integrated outcrop, 3D seismic, and geochronologic interpretation of Red Sea dike-related deformation in the Western Desert, Egypt: The role of the 23 Ma Cairo “mini-plume”: *Journal of African Earth Sciences*, v. 109, p. 107–119, <https://doi.org/10.1016/j.jafrearsci.2015.05.005>.
- Chabert, C., and Watson, R.A., 1981, Mapping and measuring caves: A conceptual analysis: *NSS Bulletin*, v. 43, p. 3–11.
- Cigna, A.A., and Forti, P., 1986, The speleogenetic role of air flow caused by convection: 1st contribution: *International Journal of Speleology*, v. 15, p. 41–52, <https://doi.org/10.5038/1827-806X.15.1.3>.
- Dasher, G.R., 1994, *On Station: A Complete Handbook for Surveying and Mapping Caves*: Huntsville, Alabama, National Speleological Society, 242 p.
- Dublyansky, Y.V., 2013, Karstification by geothermal waters, in Shroder, J. and Frumkin, A., eds., *Treatise on Geomorphology*: London, Academic Press, v. 6, p. 57–71, <https://doi.org/10.1016/B978-0-12-374739-6.00110-X>.
- Egyptian General Petroleum Corporation, 1964, Oligocene and Miocene rock stratigraphy of the Gulf of Suez region: Cairo, Consultative Stratigraphic Committee of the Egyptian General Petroleum Corporation, Report E.R. 575, 142 p.
- Egyptian Mineral Resources Authority, 2005, Geologic map of Ras Abu Bakr Quadrangle, Egypt, NH 36 B6, scale 1:100,000, 1 sheet, reproduced in Egyptian Geological Survey & Mining Authority field project no. 7196.
- Evans, A.L., 1988, Neogene tectonic and stratigraphic events in the Gulf of Suez rift area, Egypt: *Tectonophysics*, v. 153, p. 235–247, [https://doi.org/10.1016/0040-1951\(88\)90018-2](https://doi.org/10.1016/0040-1951(88)90018-2).
- Evans, A.L., 1990, Miocene sandstone provenance relations in the Gulf of Suez: Insights into synrift unroofing and uplift history: *AAPG Bulletin*, v. 74, p. 1386–1400, <https://doi.org/10.1306/0C9B24D9-1710-11D7-8645000102C1865D>.
- Fahim, W.Kh., 2015, Karst landforms in Matruh area a geomorphological study using geographic information systems techniques [M.S. thesis]: Benha University, 302 p., http://db4.eulc.edu.eg/eulc_v5/Libraries/Thesis/BrowseThesisPages.aspx?fn=PublicDrawThesis&BibID=12131195.
- Fahim, W.Kh., 2019, Karst landforms in El-Galala El-Qibliya Plateau, Eastern Desert, Egypt, using remote sensing and geographic information systems techniques [Ph.D. dissertation]: Ain Shams University, 248 p., http://srv4.eulc.edu.eg/eulc_v5/Libraries/Thesis/BrowseThesisPages.aspx?fn=PublicDrawThesis&BibID=12589968.
- Fahim, W.Kh., 2022, *The Netherworld News* (in press).
- Ford, D., and Williams, P., 2007, *Karst hydrogeology and geomorphology: West Sussex, England*, John Wiley & Sons, 562 p., <https://doi.org/10.1002/9781118684986>.
- Garfunkel, Z., 1988, Relation between continental rifting and uplifting: Evidence from the Suez rift and northern Red Sea: *Tectonophysics*, v.

- 150, p. 33–49. [https://doi.org/10.1016/0040-1951\(88\)90294-6](https://doi.org/10.1016/0040-1951(88)90294-6).
- Garfunkel, Z., and Bartov, Y., 1977, The tectonics of the Suez rift: Geological Survey of Israel Bulletin, no. 71, 44 p.
- Goodman, S.M., Hobbs, J.J., and Brewer, D.J., 1992, Nimir Cave: Morphology and fauna of a cave in the Egyptian Eastern Desert, *in* Heine, K. and Bakker, E.M.V.Z., eds., *Palaeoecology of Africa and the Surrounding Islands*, v. 23: Rotterdam, A.A. Balkema, p. 73–90.
- Griffin, D.L., 2002, Aridity and humidity: Two aspects of the late Miocene climate of North Africa and the Mediterranean: *Palaeogeography, Palaeoclimatology, Palaeoecology*, v. 182, p. 65–91, [https://doi.org/10.1016/S0031-0182\(01\)00453-9](https://doi.org/10.1016/S0031-0182(01)00453-9).
- Halliday, W.R., 2001, St. Anthony's Cave, Eastern Desert: *SpeleoDigest 2000: Huntsville Alabama*, National Speleological Society, p. 326.
- Halliday, W.R., 2002, Karst at Saint Anthony's monastery, Eastern Desert of Egypt [abstract], *in* al-Mughāwir, N.L.T., ed., *MES Symposium 2001: The Proceedings of the Middle-East Speleology Symposium, Lebanon 2001*: Kaslik, Lebanon, Speleo-Club du Liban, p. 120.
- Halliday, W.R., 2003, Caves and karsts of Northeast Africa: *International Journal of Speleology*, v. 32, p. 19–32, <https://doi.org/10.5038/1827-806X.32.1.2>.
- Hantar, G., 1965, Remarks on the distribution of the Miocene sediments in the Gulf of Suez region, *in* *Proceedings of the 5th Arab Petroleum Congress*: Cairo, p. 1–13.
- Haq, B.U., Hardenbol, J., and Vail, P.R., 1987, Chronology of fluctuating sea levels since the Triassic: *Science*, v. 235, p. 1156–1167, <https://doi.org/10.1126/science.235.4793.1156>.
- Harrell, J.A., Broekmans, M.A.T.M., and Godfrey-Smith, D.I., 2007, The origin, destruction and restoration of colour in Egyptian travertine: *Archaeometry*, v. 49, p. 421–436, <https://doi.org/10.1111/j.1475-4754.2007.00312.x>.
- Hedges, J., Russell, B., Thrun, B., and White, W.B., 1979, The 1976 NSS standard map symbols: *NSS Bulletin*, v. 41, p. 35–48.
- Hobbs, J.J., and Goodman, S.M., 1995, Leopard-hunting scenes in dated rock paintings from the northern Eastern Desert of Egypt: *Sahara*, v. 7, p. 7–16.
- Höntzsch, S., Scheibner, C., Kuss, J., Marzouk, A.M., and Rasser, M.W., 2010, Tectonically driven carbonate ramp evolution at the southern Tethyan shelf: The lower Eocene succession of the Galala Mountains, Egypt: *Facies*, v. 57, p. 51–72, <https://doi.org/10.1007/s10347-010-0229-x>.
- Hume, W.F., Madgwick, T.G., Moon, F.W., and Sadek, H., 1920, Preliminary Geological Report on Gebel Tanka Area: Cairo, Ministry of Finance, petroleum research *bulletin no. 4*, 16 p.
- Jackson, C.A.L., Gawthorpe, R.L., Leppard, C.W., and Sharp, I.R., 2006, Rift-initiation development of normal fault blocks: Insights from the Hammam Faraun fault block, Suez Rift, Egypt: *Journal of the Geological Society*, v. 163, p. 165–183, <https://doi.org/10.1144/0016-764904-164>.
- Jarrige, J.-J., d'Estevou, P.O., Burollet, P.F., Montenat, C., Prat, P., Richert, J.-P., and Thiriet, J.-P., 1990, The multistage tectonic evolution of the Gulf of Suez and northern Red Sea continental rift from field observations: *Tectonics*, v. 9, p. 441–465, <https://doi.org/10.1029/TC009i003p00441>.
- Khalil, M.M., Hamer, K., Pichler, T., and Abotalib, A.Z., 2021, Fault zone hydrogeology in arid environments: The origin of cold springs in the Wadi Araba Basin, Egypt: *Hydrological Processes*, v. 35, e14176, <https://doi.org/10.1002/hyp.14176>.
- Klimchouk, A., 2009, Morphogenesis of hypogenic caves: *Geomorphology*, v. 106, p. 100–117, <https://doi.org/10.1016/j.geomorph.2008.09.013>.
- Klimchouk, A., 2017, Types and settings of hypogene karst, *in* Klimchouk, A., Palmer, A.N., De Waele, J., Auler, A.S., and Audra, P., eds., *Hypogene Karst Regions and Caves of the World*: Cham, Switzerland, Springer, p. 1–39, https://doi.org/10.1007/978-3-319-53348-3_1.
- Klimchouk, A., 2019, Speleogenesis: Hypogene, *in* White, W. B., Culver, D. C., and Pipan, T., eds., *Encyclopedia of Caves*, 3d ed.: London, Academic Press, p. 974–988, <https://doi.org/10.1016/B978-0-12-814124-3.00114-X>.
- Klimchouk, A., Palmer, A.N., De Waele, J., Auler, A.S., and Audra, P., eds., 2017, *Hypogene Karst Regions and Caves of the World*: Cham, Switzerland, Springer, 911 p., <https://doi.org/10.1007/978-3-319-53348-3>.
- Klimchouk, A.B., 2007, Hypogene Speleogenesis: Hydrogeological and Morphogenetic Perspective: Carlsbad, N.M., National Cave and Karst Research Institute, special paper no. 1, 106 p.
- Klitzsch, E., List, F.K., Pohlmann, G., Handley, R., Hermina, M., and Meissner, B., eds., 1987, Geological map of Egypt: Conoco/Egyptian General Petroleum Corporation, NH 36 SW Beni Suef, scale 1:500 000, 1 sheet.
- Lyster, W., 1999, Monastery of St. Paul: Cairo, American Research Center in Egypt, 97 p.
- Meneisy, M.Y., 1990, Volcanicity, *in* Said, R., ed., *The Geology of Egypt*: Rotterdam, A.A. Balkema, p. 157–172, <https://doi.org/10.1201/9780203736678-9>.
- Moretti, I., and Colletta, B., 1987, Spatial and temporal evolution of the Suez rift subsidence: *Journal of Geodynamics*, v. 7, p. 151–168, [https://doi.org/10.1016/0264-3707\(87\)90069-X](https://doi.org/10.1016/0264-3707(87)90069-X).
- Moustafa, A.R., 2020, Mesozoic-Cenozoic Deformation History of Egypt, *in* Hamimi, Z., El-Barkooky, A., Martínez Frías, J., Fritz, H., and Abd El-Rahman, Y., eds., *The Geology of Egypt*: Cham, Switzerland, Springer, p. 253–294, https://doi.org/10.1007/978-3-030-15265-9_7.
- Moustafa, A.R., and Khalil, M.H., 1995, Superposed deformation in the northern Suez Rift, Egypt: Relevance to hydrocarbon exploration: *Journal of Petroleum Geology*, v. 18, p. 245–266, <https://doi.org/10.1111/j.1747-5457.1995.tb00905.x>.
- Moustafa, A.R., and Khalil, S.M., 2017, Control of extensional transfer zones on syntectonic and post-tectonic sedimentation: Implications for hydrocarbon exploration: *Journal of the Geological Society*, v. 174, p. 318–335, <https://doi.org/10.1144/jgs2015-138>.
- Moustafa, A.R., and Khalil, S.M., 2020, Structural setting and tectonic evolution of the Gulf of Suez, NW Red Sea and Gulf of Aqaba rift systems, *in* Hamimi, Z., El-Barkooky, A., Martínez Frías, J., Fritz, H., and Abd El-Rahman, Y., eds., *The Geology of Egypt*: Cham, Switzerland, Springer, p. 295–342, https://doi.org/10.1007/978-3-030-15265-9_8.
- Myroie, J.E., and Carew, J.L., 1990, The flank margin model for dissolution cave development in carbonate platforms: *Earth Surface Processes and Landforms* v. 15, p. 413–424, <https://doi.org/10.1002/esp.3290150505>.
- Omar, G.I., Steckler, M.S., Buck, W.R., and Kohn, B.P., 1989, Fission-track analysis of basement apatites at the western margin of the Gulf of Suez rift, Egypt: Evidence for synchronicity of uplift and subsidence: *Earth and Planetary Science Letters*, v. 94, p. 316–328, [https://doi.org/10.1016/0012-821X\(89\)90149-0](https://doi.org/10.1016/0012-821X(89)90149-0).
- Palmer, A.N., 1991, Origin and morphology of limestone caves: *Geological Society of America Bulletin*, v. 103, p. 1–21, [https://doi.org/10.1130/0016-7606\(1991\)103<0001:OAMOLC>2.3.CO;2](https://doi.org/10.1130/0016-7606(1991)103<0001:OAMOLC>2.3.CO;2).
- Palmer, A.N., 2007, *Cave Geology*: Dayton, Ohio, Cave Books, 454 p.
- Patton, T.L., Moustafa, A.R., Nelson, R.A., and Abdine, S.A., 1994, Tectonic evolution and structural setting of the Suez Rift, *in* Landon, S.M., ed., *Interior Rift Basins*: Tulsa, American Association of Petroleum Geologists, memoir 59, p. 9–55, <https://doi.org/10.1306/M59582C2>.
- Peijs, J.A.M.M., Bevan, T.G., and Piombino, J.T., 2012, The Gulf of Suez rift basin, *in* Roberts, D.G., and Bally, A.W., eds., *Regional Geology and*

- Tectonics: Phanerozoic Rift Systems and Sedimentary Basins, v. 1B, Amsterdam, Elsevier, p. 165–194, <https://doi.org/10.1016/B978-0-444-56356-9.00007-9>.
- Richardson, M., and Arthur, M.A., 1988, The Gulf of Suez-northern Red Sea neogene rift: A quantitative basin analysis: *Marine and Petroleum Geology*, v. 5, p. 247–270, [https://doi.org/10.1016/0264-8172\(88\)90005-0](https://doi.org/10.1016/0264-8172(88)90005-0).
- Robson, D.A., 1971, The structure of the Gulf of Suez (Clysmic) rift, with special reference to the eastern side: *Journal of the Geological Society*, v. 127, p. 247–276, <https://doi.org/10.1144/gsjgs.127.3.0247>.
- Rubenson, S., 2016, Excavations at the Monastery of St. Antony at the Red Sea: The monastery in literary sources during the period of study: *Opuscula*, v. 9, p. 209–211, <https://www.doi.org/10.30549/opathrom-09-07>.
- Said, R., 1962, *The Geology of Egypt*: Amsterdam, Elsevier Publishing, 377 p.
- Scheibner, C., Marzouk, A.M., and Kuss, J., 2001, Maastrichtian-Early Eocene litho-biostratigraphy and palaeogeography of the northern Gulf of Suez region, Egypt: *Journal of African Earth Sciences*, v. 32, p. 223–255, [https://doi.org/10.1016/S0899-5362\(01\)90005-3](https://doi.org/10.1016/S0899-5362(01)90005-3).
- Schoeller, H., 1962, *Les Eaux Souterraines: Hydrologie Dynamique et Chimique: Recherche, Exploitation, et Évaluation des Ressources* [Groundwater: Dynamic and Chemical Hydrology: Research, Use, and Resource Evaluation]: Paris, Masson & Cie, 642 p.
- Schütz, K.I., 1994, Structure and stratigraphy of the Gulf of Suez, Egypt, *in* Landon, S.M., ed., *Interior Rift Basins*: Tulsa, American Association of Petroleum Geologists, Memoir 59, p. 57–96, <https://doi.org/10.1306/M59582C3>.
- Sibson, R.H., 1996, Structural permeability of fluid-driven fault-fracture meshes: *Journal of Structural Geology*, v. 18, p. 1031–1042, [https://doi.org/10.1016/0191-8141\(96\)00032-6](https://doi.org/10.1016/0191-8141(96)00032-6).
- Steckler, M.S., Berthelot, F., Lyberis, N., and LePichon, X., 1988, Subsidence in the Gulf of Suez: Implications for rifting and plate kinematics: *Tectonophysics*, v. 153, p. 249–270, [https://doi.org/10.1016/0040-1951\(88\)90019-4](https://doi.org/10.1016/0040-1951(88)90019-4).
- Steen, G., 1984, Radiometric age dating and tectonic significance of some Gulf of Suez igneous rocks, *in* Proceedings, 6th Exploration Seminar, March 1982: Cairo, Egyptian General Petroleum Corporation and Egypt Petroleum Exploration Society, v. 1, p. 199–211.
- Sturchio, N.C., Arehart, G.B., Sultan, M., Sano, Y., AboKamar, Y., and Sayed, M., 1996, Composition and origin of thermal waters in the Gulf of Suez area, Egypt: *Applied Geochemistry*, v. 11, p. 471–479, [https://doi.org/10.1016/0883-2927\(96\)00025-X](https://doi.org/10.1016/0883-2927(96)00025-X).
- Tourre, S.A., 2000, *Cave-filling herringbone calcite: Morphology and geochemistry of an unusual carbonate cement from Egypt* [M.S. dissertation], University of California, Davis, 61 leaves.
- Wannous, M., Theilen-Willige, B., Troeger, U., Falk, M., Siebert, C., and Bauer, F., 2021, Hydrochemistry and environmental isotopes of spring water and their relation to structure and lithology identified with remote sensing methods in Wadi Araba, Egypt: *Hydrogeology Journal*, v. 29, p. 2245–2266, <https://doi.org/10.1007/s10040-021-02343-x>.